Available online at www.sciencedirect.com
ScienceDirect
Journal of Magnetic Resonance 191 (2008) 31–46
JMR Journal of Magnetic Resonance
www.elsevier.com/locate/jmr

The effectiveness of ^{1}H decoupling in the ^{13}C MAS NMR of paramagnetic solids: An experimental case study incorporating copper(II) amino acid complexes

Mathew J. Willans, Devin N. Sears, Roderick E. Wasylishen *

Department of Chemistry, University of Alberta, Edmonton, Alta., Canada T6G 2G2

Received 14 September 2007; revised 17 November 2007
Available online 20 December 2007

Abstract

The use of continuous-wave (CW) ^{1}H decoupling has generally provided little improvement in the ^{13}C MAS NMR spectroscopy of paramagnetic organic solids. Recent solid-state ^{13}C NMR studies have demonstrated that at rapid magic-angle spinning rates CW decoupling can result in reductions in signal-to-noise and that ^{1}H decoupling should be omitted when acquiring ^{13}C MAS NMR spectra of paramagnetic solids. However, studies of the effectiveness of modern ^{1}H decoupling sequences are lacking, and the performance of such sequences over a variety of experimental conditions must be investigated before ^{1}H decoupling is discounted altogether. We have studied the performance of several commonly used advanced decoupling pulse sequences, namely the TPPM, SPINAL-64, XiX, and eDROOPY sequences, in ^{13}C MAS NMR experiments performed under four combinations of the magnetic field strength (7.05 or 11.75 T), rotor frequency (15 or 30 kHz), and ^{1}H rf-field strength (71, 100, or 140 kHz). The effectiveness of these sequences has been evaluated by comparing the ^{13}C signal intensity, linewidth at half-height, LWHH, and coherence lifetimes, T_2', of the methine carbon of copper(II) bis(DL-alanine) monohydrate, $Cu(ala)_2{\cdot}H_2O$, and methylene carbon of copper(II) bis(DL-2-aminobutyrate), $Cu(ambut)_2$, obtained with the advanced sequences to those obtained without ^{1}H decoupling, with CW decoupling, and for fully deuterium labelled samples. The latter have been used as model compounds with perfect ^{1}H decoupling and provide a measure of the efficiency of the ^{1}H decoupling sequence. Overall, the effectiveness of ^{1}H decoupling depends strongly on the decoupling sequence utilized, the experimental conditions and the sample studied. Of the decoupling sequences studied, the XiX sequence consistently yielded the best results, although any of the advanced decoupling sequences strongly outperformed the CW sequence and provided improvements over no ^{1}H decoupling. Experiments performed at 7.05 T demonstrate that the XiX decoupling sequence is the least sensitive to changes in the ^{1}H transmitter frequency and may explain the superior performance of this decoupling sequence. Overall, the most important factor in the effectiveness of ^{1}H decoupling was the carbon type studied, with the methylene carbon of $Cu(ambut)_2$ being substantially more sensitive to ^{1}H decoupling than the methine carbon of $Cu(ala)_2{\cdot}H_2O$. An analysis of the various broadening mechanisms contributing to ^{13}C linewidths has been performed in order to rationalize the different sensitivities of the two carbon sites under the four experimental conditions.

Keywords: Heteronuclear decoupling; ^{13}C solid-state NMR spectroscopy; Paramagnetic metal-organic complexes; Copper; Amino acids

1. Introduction

Experimental approaches to obtain high-resolution carbon-13 NMR spectra of diamagnetic organic solids have been well-established, and three essential solid-state NMR techniques are consistently utilized: ^{1}H–^{13}C cross-polarization, magic-angle spinning, MAS, and ^{1}H (high-power heteronuclear) decoupling [1,2]. Cross-polarization enhances the ^{13}C magnetization and decreases the experimental recycle delay, thereby significantly reducing total experiment times [3,4]. Magic-angle spinning, MAS, averages the orientation-dependent ^{13}C magnetic shielding and ^{13}C-dilute-spin dipolar coupling interactions, leading

* Corresponding author. Fax: +1 780 492 8231.
E-mail address: roderick.wasylishen@ualberta.ca (R.E. Wasylishen).

1090-7807/$ - see front matter © 2007 Elsevier Inc. All rights reserved.
doi:10.1016/j.jmr.2007.11.012

to spectra with peaks corresponding only to the different isotropic chemical shifts [5–7]. High-power ^{1}H decoupling removes a large portion of ^{13}C–^{1}H dipolar interactions that are not fully averaged by MAS alone, resulting in considerable line-narrowing and a resultant increase in resolution and signal-to-noise [8,9].

The use of the above NMR techniques to acquire ^{13}C NMR spectra of organic free radicals or paramagnetic metal-organic complexes; however, has generally resulted in ^{13}C NMR spectra having poor signal-to-noise and limited resolution [10–42]. This has brought into question whether the combination of the above techniques provides the best method by which to acquire high-resolution ^{13}C NMR spectra of paramagnetic solids. In particular, the usefulness and effectiveness of ^{1}H decoupling has been questioned on several occasions [19,23,26–28,38,41,42], the poor decoupling performance in paramagnetic solids generally being attributed to the large ^{1}H chemical shift dispersion and anisotropies that prevent ''on-resonance'' decoupling. Recently, it has been shown that at rapid MAS rates, decoupling can be omitted without loss of resolution, which in-turn drastically reduces the experimental duty cycle and allows one to utilize very short recycle delays afforded by rapid nuclear relaxation times in paramagnetic solids [38,42].

All of the previously mentioned studies; however, appear to have utilized continuous-wave (CW) ^{1}H decoupling, a ^{1}H decoupling sequence that has been supplanted by numerous multi-pulse decoupling sequences [43–56]. While it is well known that these advanced decoupling sequences strongly outperform CW decoupling when acquiring ^{13}C MAS NMR spectra of diamagnetic organic solids, it is not known whether advanced sequences provide similar improvements for paramagnetic solids. Thus, we have investigated the performance of several commonly used advanced ^{1}H heteronuclear decoupling sequences, specifically TPPM [43], SPINAL-64 [46], XiX [49], and eDROOPY [50], in the ^{13}C solid-state NMR spectra of copper(II) bis(DL-alanine) monohydrate, $Cu(ala)_2{\cdot}H_2O$, and copper(II) bis(DL-2-aminobutyrate), $Cu(ambut)_2$. Evaluation of the decoupling sequences is based on comparisons of the ^{13}C signal intensities, linewidths at half-height, LWHH, and coherence lifetimes, T_2' [57,58] of the methine carbon of $Cu(ala)_2{\cdot}H_2O$ and the methylene carbon of $Cu(ambut)_2$ obtained with ^{1}H decoupling and without ^{1}H decoupling over a range of experimental conditions: applied magnetic fields of 7.05 and 11.75 T, spinning rates of 15 and 30 kHz, and radiofrequency, rf, decoupling fields, $\nu_1(^{1}H)$, of 71, 100 and 140 kHz. Using fully deuterated samples, the efficiency of the various pulse sequences have been estimated. A discussion of the performance of the ^{1}H decoupling sequences follows, in which the results have been rationalized using current ^{1}H decoupling theory, by monitoring the ^{1}H decoupler offset, and from an evaluation of the various broadening mechanisms that contribute to the ^{13}C linewidths.

2. Methodology and experimental details

2.1. Synthesis

Copper(II) bis(DL-alanine) hydrate was synthesized via the reaction of a solution of DL-alanine (Aldrich) and an equimolar amount of potassium hydroxide (Fisher) in distilled water with a solution of copper(II) chloride dihydrate (Aldrich) in distilled water. Copper(II) chloride dihydrate was present in a slight excess over the stoichiometric ratio. The reaction was allowed to proceed for several hours and the solution was evaporated to dryness overnight. The resulting solid was washed with distilled water and filtered. The product was then dried in air for several hours. This procedure was repeated for the synthesis of copper(II) bis(DL-alanine-2-^{13}C) hydrate using DL-alanine-2-^{13}C (99% ^{13}C, CIL). For the synthesis of copper(II) bis(DL-alanine-2,3,3,3-d_4-N-d_2)·D_2O, DL-alanine-2,3,3,3-d_4 (99.3% D, C/D/N Isotopes), KOH and $CuCl_2{\cdot}2H_2O$ were each first dissolved in D_2O (99.8% D, CIL) and allowed to recrystallize three times. The copper complex was then synthesized as described above under nitrogen gas using standard Schlenk-line techniques and the product was washed with D_2O.

Copper(II) bis(DL-2-aminobutyrate), copper(II) bis(DL-2-aminobutyrate-3-^{13}C), and copper(II) bis(DL-2-aminobutyrate-2,3,3,4,4,4-d_6-N-d_2) were synthesized in the same manner as above using DL-2-aminobutyric acid (Aldrich), DL-2-aminobutyric-3-^{13}C acid (99% ^{13}C, Icon Isotopes), and DL-2-aminobutyric-2,3,3,4,4,4-d_6 acid (98.8% D, C/D/N isotopes), respectively.

2.2. Solid-state ^{13}C and ^{1}H NMR spectroscopy

Of the various carbon bonding environments in a saturated organic molecule, quaternary carbons possess no directly bonded hydrogen atoms and are the easiest to decouple. Methyl groups are more difficult, although partial averaging of the ^{13}C–^{1}H heteronuclear dipolar coupling by rapid rotation of the hydrogen atoms about the methyl groups local C_3-axis generally makes methyl carbons slightly easier to decouple than methine carbons. Methylene carbons are the most difficult to decouple due the large homonuclear dipolar coupling between the two adjacent hydrogen atoms. Thus, we chose both a methine and methylene carbon containing paramagnetic complex for this study. $Cu(ala)_2{\cdot}H_2O$ has been used by several researchers in the past as a model compound [27,38,42] and was selected as the methine carbon containing compound for this study; $Cu(ambut)_2$ was selected as the methylene carbon containing compound.

Although there are numerous multiple-pulse ^{1}H heteronuclear decoupling pulse sequences designed for solid-state NMR, the TPPM [43], SPINAL-64 [46], XiX [49], and eDROOPY [50] sequences seem to have attracted the most attention and have been selected for this study. In addition, CW decoupling has been included for comparison and

completeness. The effectiveness of the ^{1}H heteronuclear decoupling sequences depends on several experimental factors: the applied magnetic field strength, the MAS rate, the ^{1}H rf-field strength, $\nu_1(^1\mathrm{H})$, the ^{1}H decoupler frequency, and the rf-field homogeneity (which, in-turn is dictated by the coil diameter and coil characteristics). While the choice of the applied magnetic field strength is generally dictated by what is available to the experimentalist and the rf-field homogeneity is characteristic of the probe, the MAS rate, ^{1}H rf-field strength, and ^{1}H decoupler frequency must be decided upon by the experimentalist. Furthermore, parameters specific to the ^{1}H decoupling sequence: the pulse width and phase difference for TPPM, the pulse width for SPINAL-64, the ratio of the pulse width to the rotor period for XiX, and the pulse width and phase difference for eDROOPY, must also be optimized by the experimentalist to achieve maximum decoupling efficiency. These parameters in-turn depend on the MAS rate, the ^{1}H rf-field strength, and the probe used.

The parameters for the ^{1}H decoupling sequences for the CH and CH_2 carbon sites were optimized on diamagnetic DL-alanine and DL-2-aminobutyric acid samples, respectively, using the same MAS rate, ^{1}H rf-field strength and probe as the corresponding ^{13}C NMR experiments on the copper(II) complexes. Note that for all experiments using TPPM decoupling, the phase difference was set to 15° and only the pulse width was optimized. The pulse widths for TPPM and SPINAL-64 decoupling sequences were obtained from optimizations in which the pulse width was varied in 0.01 μs steps. The ratio of the pulse width to the rotor period required for optimum XiX decoupling was obtained by varying this ratio in increments of ±0.01 about 2.86. The pulse width and phase difference needed for eDROOPY were obtained using a simplex minimization routine [50] that was originally downloaded from the website of Prof. Lyndon Emsley (http://www.ens-lyon.fr/CHIMIE/Fr/Groupes/NMR/Pages/library.html) and was subsequently modified for our spectrometers. The modified code can be found on the website of Prof. Paul Hodgkinson (http://www.dur.ac.uk/paul.hodgkinson/software/index.html).

In this study, we have investigated the performance of the ^{1}H decoupling sequences over a wide range of experimental parameters at applied magnetic field strengths of 7.05 and 11.75 T. At the low magnetic field strength, experiments were performed on a Bruker Avance 300 NMR spectrometer with a Bruker MAS probe utilizing 4 mm o.d. ZrO_2 rotors. Two ^{1}H decoupling field strengths were used, 71 kHz (3.5 μs ^{1}H π/2 pulse) and 100 kHz (2.5 μs ^{1}H π/2 pulse), the latter being the maximum specification for the probe. The spinning rate was set to the maximum for the probe, 15 kHz, in order to minimize complications from the presence of spinning sidebands. To gauge the applied magnetic field dependence of ^{1}H decoupling, the experiments with $\nu_1(^1\mathrm{H}) = 100$ kHz and spinning rate of 15 kHz were repeated at 11.75 T on a Bruker Avance 500 NMR spectrometer. Additionally, NMR spectra at 11.75 T were obtained using a probe that utilized 2.5 mm o.d. rotors; the rotor frequency was set to 30 kHz and the ^{1}H rf-field to 140 kHz (maximum recommended for the probe). Unless otherwise specified, the ^{1}H decoupling frequency was set to correspond to the frequency of the most intense peak in the ^{1}H spectrum and this was considered the "on-resonance" condition.

In order to minimize first-order phase corrections and baseline distortions caused by the rapid dephasing of ^{13}C magnetization in paramagnetic solids, the ^{13}C NMR spectra were obtained using a spin-echo, $(\pi/2)_x - \tau_1 - \pi_y - \tau_2$-acq, pulse sequence. The initial delay, τ_1, was set to 66.67 μs ($1/\nu_{\mathrm{rot}} = 1/15{,}000$ Hz), whether ν_{rot} was 15 or 30 kHz, and the second delay, τ_2, was optimized to ensure all points in the FID were collected. C-13 coherence lifetimes, T_2's, were determined by fitting the signal intensities, $S(\tau)$, from between 23 and 29 spin-echo experiments, in which τ_1 and τ_2 were varied in integer multiples of $1/\nu_{\mathrm{rot}}$, to the equation $S(2\tau) = S_0 * \exp(-2\tau/T_2')$ [59,60]. Fitting and error analysis was performed using the program SigmaPlot 2001. All ^{13}C chemical shifts were referenced with respect to TMS ($\delta(^{13}\mathrm{C}) = 0.0$ ppm) by setting the high-frequency reference of adamantane to 38.56 ppm. H-1 spectra were acquired with a 1-pulse sequence with a 1 second recycle delay, collecting 64–256 transients using a 3.0 μs ($\nu_1 = 83.3$ kHz) excitation pulse, and were referenced with respect to TMS ($\delta(^1\mathrm{H}) = 0.0$ ppm) by setting the OH resonance of MeOH-d_4 to 4.78 ppm.

The ^{13}C NMR spectra of DL-alanine and DL-2-aminobutyric acid were obtained using a spin-echo sequence preceded by cross-polarization with a tangential amplitude sweep on the ^{13}C channel.[20] A 5 second recycle delay was used and 512 transients were collected. With the 4 mm probe, a 4.0 μs ^{1}H π/2 pulse with a 0.7 ms contact time for DL-alanine and 3.5 ms contact time for DL-2-aminobutyric acid was utilized. The same parameters were used with the 2.5 mm probe except the initial ^{1}H pulse was decreased to 3.0 μs.

3. Results

3.1. ^{1}H MAS NMR spectroscopy

The first step in optimizing a ^{13}C NMR experiment is to acquire a ^{1}H MAS NMR spectrum. This provides the experimentalist with the approximate bandwidth and decoupler offset frequency necessary for efficient ^{1}H decoupling. The ^{1}H MAS NMR spectra of $Cu(ala)_2{\cdot}H_2O$ and $Cu(ambut)_2$ at the different applied magnetic field strengths and spinning rates utilized in this study are presented in Figs. 1 and 2, respectively. Unlike the ^{1}H MAS NMR spectra of diamagnetic molecules the ^{1}H MAS NMR spectrum of $Cu(ala)_2{\cdot}H_2O$ at $B_o = 7.05$ T shows distinct isotropic peaks due to large paramagnetic shifts [27]. Utilizing ^{1}H and ^{2}H spectroscopy of ^{2}H labelled samples in the same manner as Liu et al. [27], the ^{1}H chemical shifts have been assigned at the experimental temperature of 51 °C and are

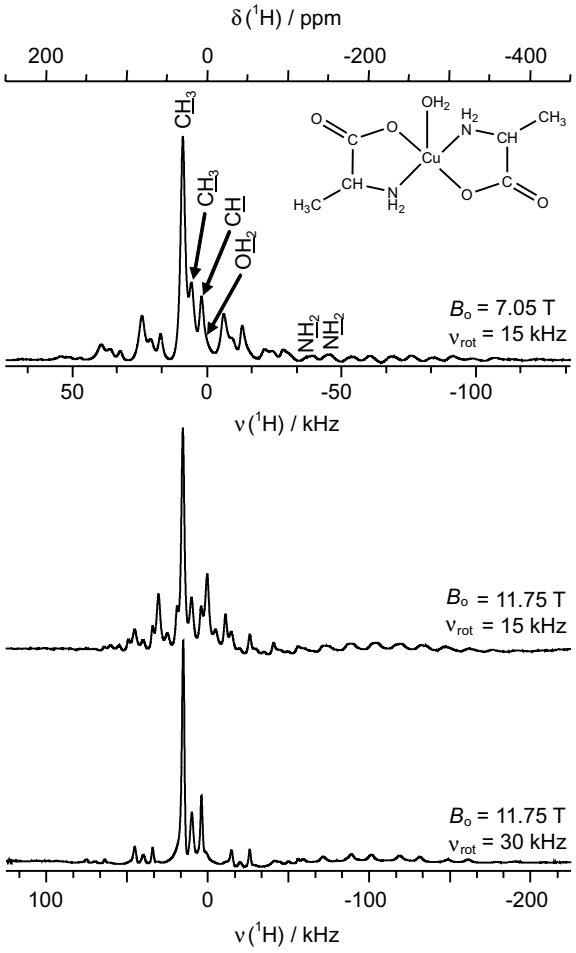

Fig. 1. ^{1}H MAS NMR spectra of Cu(DL-alanine)$_2$·H$_2$O obtained under various experimental conditions.

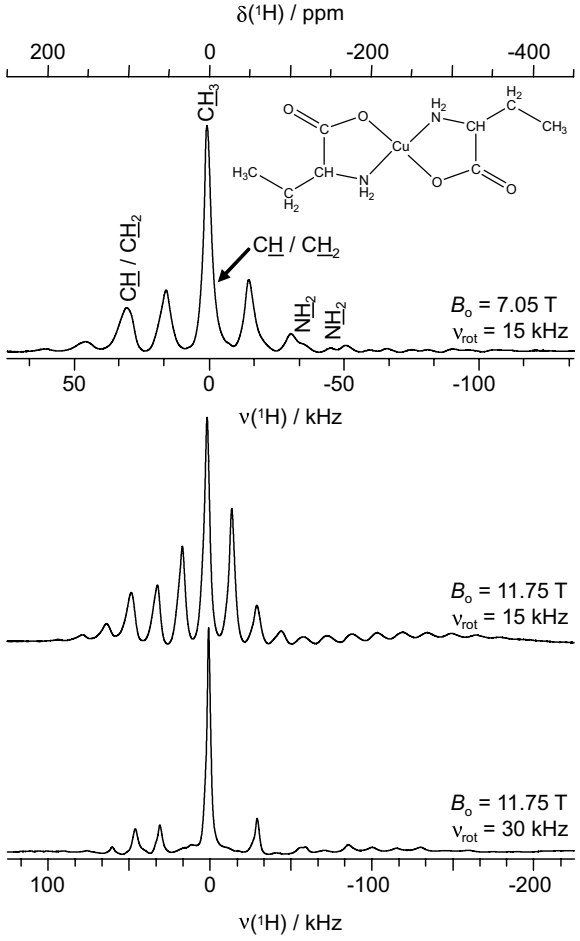

Fig. 2. ^{1}H MAS NMR spectra of Cu(DL-2-aminobutyrate)$_2$ obtained under various experimental conditions.

spread over 55 kHz at an applied magnetic field of 7.05 T: $\delta_{iso}(CH_3) = 30$ and 19 ppm, $\delta_{iso}(CH) = 6$ ppm, $\delta_{iso}(NH_2) = -122$ and -149 ppm, and $\delta_{iso}(H_2O) = 1$ ppm. In addition to the large ^{1}H chemical shift dispersion in Cu(ala)$_2$·H$_2$O, there are numerous spinning sidebands evident in the spectrum that span about 150 kHz at $B_o = 7.05$ T. The spinning sidebands result not just from the dipolar coupling between ^{1}H nuclei, as in diamagnetic solids, but also from the large orientation-dependence of the dipolar shift (pseudocontact shift) that results from the presence of the unpaired electron. The largest spinning sideband manifold likely arises from the two NH_2 sites in close proximity to the unpaired electron localized predominantly at the Cu(II) centre.

At an applied magnetic field of 11.75 T, the ^{1}H spectrum of Cu(ala)$_2$·H$_2$O is spread over a much larger frequency range, nearly 250 kHz, while the isotropic chemical shifts are spread over about 90 kHz (Fig. 1, middle and bottom panel). The advantages of spinning fast when acquiring ^{1}H solid-state NMR spectra are clearly evident in the spectra acquired with a spinning rate of 30 kHz. Many of the spinning sidebands have been removed and the isotropic chemical shifts can be much more readily identified. In this spectrum, the low intensity water resonance is just detectable and appears as a low-frequency shoulder to the three large peaks centred about 20 ppm. Minor changes in the ^{1}H chemical shifts were observed from the spectra obtained with $\nu_{rot} = 15$ kHz due to the slightly higher sample temperature of 64 °C with $\nu_{rot} = 30$ kHz.

For Cu(ambut)$_2$, the ^{1}H/^{2}H chemical shifts had not been previously assigned and selectively ^{2}H labelled 2-aminobutyric acid is not commercially available. Using the combination of full deuterium labelling and both ^{1}H and ^{2}H NMR spectroscopy, there are isotropic ^{1}H chemical shifts at 96, 3, 0 (shoulder to the peak at 3 ppm), -116, and -148 ppm. From Cu(ala)$_2$·H$_2$O, the two low-frequency peaks ($\delta_{iso} = -116$, and -148 ppm) can be assigned to the NH_2 peaks. The CH_3 resonances should be the most intense and least shifted in comparison to the free ligand, and thus likely corresponds to the most intense peak at 3 ppm. The methylene and methine ^{1}H NMR peaks could not be assigned. Similar to Cu(ala)$_2$·H$_2$O, the complete ^{1}H NMR spectrum of Cu(ambut)$_2$ is spread over nearly 150 kHz at 7.05 T and about 250 kHz at 11.75 T (Fig. 2). The NH_2 peaks are difficult to observe and have low relative intensity. Unlike Cu(ala)$_2$·H$_2$O, two of the ^{1}H peaks in

$Cu(ambut)_2$ overlap and much of the intensity in the ^1H spectra is within these two peaks.

The relatively large isotropic ^1H chemical shift dispersion and chemical shift anisotropies present in the compounds studied makes decoupling more demanding than in typical diamagnetic compounds. First, a large decoupling bandwidth of about 150 kHz at 7.05 T and 250 kHz at 11.75 T is needed for efficient decoupling. Second, the ^1H frequencies of the spins depend significantly on the orientation of the crystallite with respect to the magnetic field, making decoupling "on-resonance" difficult to achieve. Third, the placement of the ^1H transmitter for optimum decoupling is not obvious, as it is for diamagnetic solids. The above complications have been used to explain the inefficient decoupling previously noted in the ^{13}C NMR spectra of paramagnetic organic solids.

3.2. ^{13}C MAS NMR spectroscopy

The influence of ^1H decoupling on the ^{13}C signal intensities of both the diamagnetic amino acids and the paramagnetic copper-amino acid complexes will be presented first (Section 3.2.1). H-1 decoupling effects on the ^{13}C linewidths (Section 3.2.2) and coherence lifetimes (Section 3.2.3) for the paramagnetic complexes will be presented afterwards. Intensity, linewidth and relaxation data are also presented for fully deuterium labelled samples. These samples are considered to have "perfect" ^1H decoupling due to the much smaller magnetogyric ratio of deuterium ($\gamma(^1H)/\gamma(^2H) = 6.514$), which results in a dramatically decreased dipolar coupling interaction between the ^{13}C and ^2H nuclei. Note that any residual ^{13}C–^2H dipolar coupling present will result in only slight broadening of the ^{13}C NMR spectra, the effect of which decreases as the magnetic field strength increases [61]. Last, for the remainder of the paper, the various experimental conditions for the ^1H decoupling experiments described in Section 2.2 will be referred to as conditions A through D and are summarized in Table 1.

3.2.1. Influence of ^1H decoupling on ^{13}C signal intensities

The effect of ^1H decoupling on the signal intensity, measured relative to no ^1H decoupling, of the methine carbon of DL-alanine (Fig. 3A) and $Cu(ala\text{-}2\text{-}^{13}C)_2{\cdot}H_2O$ (Fig. 3B) at both 7.05 and 11.75 T is presented in Fig. 3. Note that for a particular decoupling condition, the noise in each ^{13}C NMR spectrum remained the same regardless of the ^1H decoupling sequence used and therefore changes in the signal intensity mimic changes in the signal-to-noise. For DL-alanine, under decoupling condition A, significant enhancement in the ^{13}C signal was observed with all of the decoupling sequences, with SPINAL-64 decoupling providing the greatest increase. With the exception of the XiX sequence, all of the advanced sequences strongly outperformed CW decoupling. When the decoupling power was increased from 71 to 100 kHz (condition B), as expected [9,50,53,62,63] the efficiency of all the decoupling sequences improved. Still, the maximum signal was achieved with SPINAL-64 decoupling and XiX performed the worst of the advanced sequences. Upon moving to $B_o = 11.75$ T, but changing no other decoupling parameters (condition C), the signal intensity decreased relative

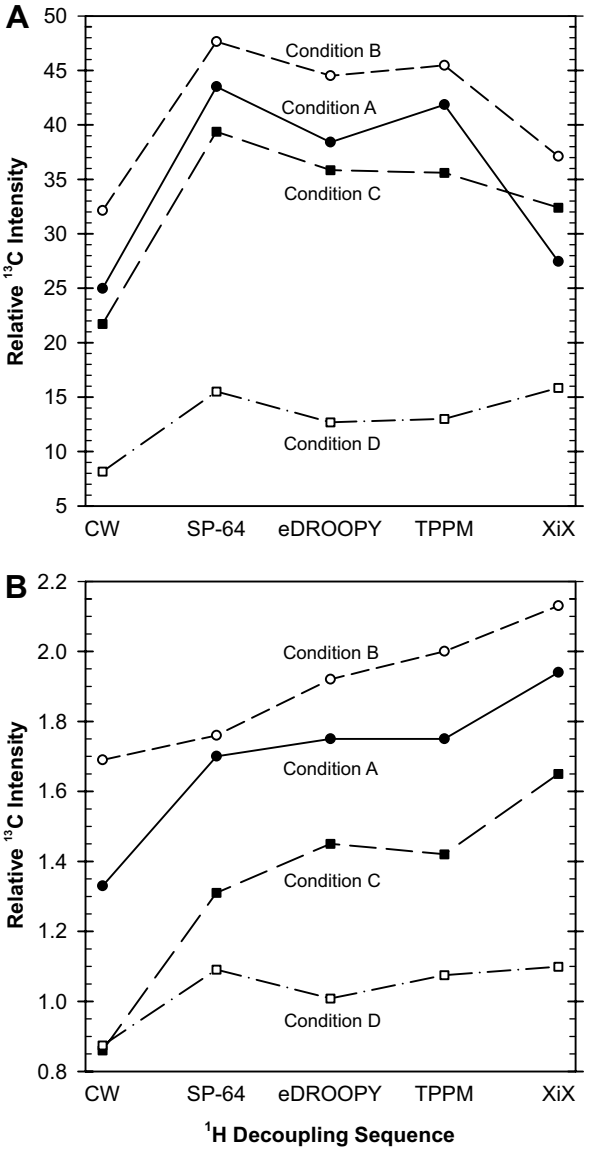

Fig. 3. (A) Plot of ^{13}C signal intensity of the methine carbon of DL-alanine and (B) $Cu(DL\text{-}alanine\text{-}2\text{-}^{13}C)_2{\cdot}H_2O$ under the experimental conditions outlined in Table 1. The ^{13}C signal intensities for each compound are plotted relative to the ^{13}C signal intensity for that compound obtained without ^1H decoupling (set to 1.0).

Table 1
Experimental conditions utilized in this study

Condition	B_o/T	ν_{rot}/kHz	$\nu_1(^1H)$/kHz	Rotor o.d./mm
A	7.05	15	71	4
B	7.05	15	100	4
C	11.75	15	100	4
D	11.75	30	140	2.5

to condition B for all sequences except XiX sequence. Last, the intensity increase upon the inclusion of decoupling is greatly reduced for condition D ($\nu_{rot} = 30$ kHz, $\nu_1(^1H) = 140$ kHz) as opposed to conditions A-C. The greatest signal increase is now obtained when XiX decoupling is used, although similar enhancements are achieved with either XiX or SPINAL-64 decoupling.

For Cu(ala-2-$^{13}C)_2{\cdot}H_2O$, the inclusion of ^1H decoupling resulted in only modest gains in signal intensity (Fig. 3B) and the relative effectiveness of the ^1H sequences differed significantly from that observed in alanine (Fig. 3A). For example, when using CW decoupling under condition A, the ^{13}C NMR peak due to the methine group increased only 1.3 times relative to no ^1H decoupling. SPINAL-64 decoupling, which performed best for alanine, provides the least signal gain of the advanced sequences. Surprisingly, XiX, which barely outperformed CW for alanine, provided the maximum relative signal increase of 1.95. With more intense decoupling fields (condition B), greater decoupling efficiency was observed but the relative performance of the ^1H decoupling sequences remained the same. Using the same spinning rate and decoupling power as with $B_o = 7.05$ T, a decrease in the effectiveness of ^1H decoupling for all ^1H decoupling sequences is realized at 11.75 T in Cu(ala-2-$^{13}C)_2{\cdot}H_2O$ (condition C). With CW decoupling, as has been observed previously [38,42], the ^{13}C signal intensity actually dropped relative to no ^1H decoupling. Under condition D, again a decrease in ^{13}C signal intensity is observed when CW decoupling is utilized and the maximum signal is obtained with XiX decoupling. This signal intensity, however, is only 1.1 times that of a ^{13}C NMR spectrum obtained without ^1H decoupling.

In order to compare signal intensities to that of the deuterated compound, ^{13}C spectra of a natural abundance sample of $Cu(ala)_2{\cdot}H_2O$ (Fig. 4) have been acquired. The natural abundance sample was used because a commercial sample of alanine with full deuterium labelling and only methine carbon ^{13}C enrichment was not available. Due to the long experimental time required to achieve an acceptable signal-to-noise in the ^{13}C NMR spectra of the natural abundance samples with the use of minimal line broadening, experiments were performed with no ^1H decoupling and the best ^1H decoupling sequence (XiX) under conditions B, C, and D (Fig. 4). For the methine carbon ($\delta_{iso} = -280$ ppm), under condition B we have already established that the inclusion of XiX decoupling doubles the intensity of this peak relative to a ^{13}C spectrum acquired without decoupling (Fig. 4, top row). Upon deuteration, there is a minor increase in signal intensity, suggesting that the ^1H decoupling is very efficient for this carbon in $Cu(ala)_2{\cdot}H_2O$. For the methyl carbon ($\delta_{iso} = 177$ ppm), where the protons are easier to decouple than in a methine group, the inclusion of ^1H decoupling resulted in a signal increase of 1.3, whereas the intensity of the carboxylate carbon ($\delta_{iso} = -198$ ppm), which has no attached protons, did not improve noticeably with the inclusion of decoupling. Upon deuteration, no appreciable change in signal intensity between the two spectra are observed for either the methyl or carboxylate carbons.

At $B_o = 11.75$ T and spinning at 15 kHz (condition C, middle row of Fig. 4), spinning sidebands are now prominant for the carboxylate and methine group carbons, showing the scaling of the chemical shift/paramagnetic shift anisotropy with the magnetic field. In comparison to condition B, smaller increases in the methyl carbon and methine carbon signal intensities are observed with the use of XiX decoupling and greater increases in the signal intensities of these carbon atoms occur upon deuterium labelling. This is further evidence that the decoupling is less efficient at higher magnetic field strengths.

For the ^{13}C spectra obtained with $\nu_{rot} = 30$ kHz (condition D, bottow row of Fig. 4), the decrease in signal-to-noise upon using the much smaller 2.5 mm rotors is clearly evident. A benefit, however, of the smaller rotors is the faster spinning rate allowed and consequently the spinning sidebands of the carboxylate peak present with $\nu_{rot} = 15$ kHz are essentially removed when the spinning rate is doubled. Under condition D, the increase in signal-to-noise observed when XiX decoupling is utilized is considerably less than observed under condition B or C. This indicates that either the ^1H decoupling is performing poorly when the spinning rate is 30 kHz or that the ^{13}C–^1H dipolar interaction is being more effectively averaged by the increased spinning rate alone. Since the observed increase in the intensity of the methine carbon peak upon deuteration is similar in magnitude to what was observed under conditions B and C, the latter is therefore true. That is, XiX decoupling is efficient under these experimental conditions but the small sensitivity to decoupling results from significant decoupling that is occurring by the fast spinning alone. This observation is in agreement with past studies that have shown that with rapid spinning rates ^1H decoupling is not essential in order to obtain high-resolution spectra of $Cu(ala)_2{\cdot}H_2O$ [38,42]. Unfortunately the decrease in signal-to-noise that results from the loss of sample volume using smaller rotors, even though the spectra with the 2.5 mm rotors were acquired with 4 times as many scans, is a major disadvantage.

The ^{13}C intensities of the methylene carbon in 2-aminobutyric acid and Cu(ambut-3-$^{13}C)_2$ are presented in Fig. 5. Not surprisingly, the same trends observed for alanine are also observed for 2-aminobutyric acid (Fig. 5A). That is, large increases in ^{13}C signal intensity are observed when ^1H decoupling is utilized (maximum of nearly 50 times), greater decoupling efficiency is obtained when the decoupling power is increased (condition A vs. B), SPINAL-64 provided the greatest increase in signal except for condition D where XiX performed the best, the decoupling effectiveness decreased as the applied magnetic field strength increased and the ^{13}C NMR intensities are the least sensitive to ^1H decoupling when spinning at 30 kHz (condition D).

The intensity of the ^{13}C NMR peak from the methylene carbon in Cu(ambut-3-$^{13}C)_2$ is much more sensitive to ^1H

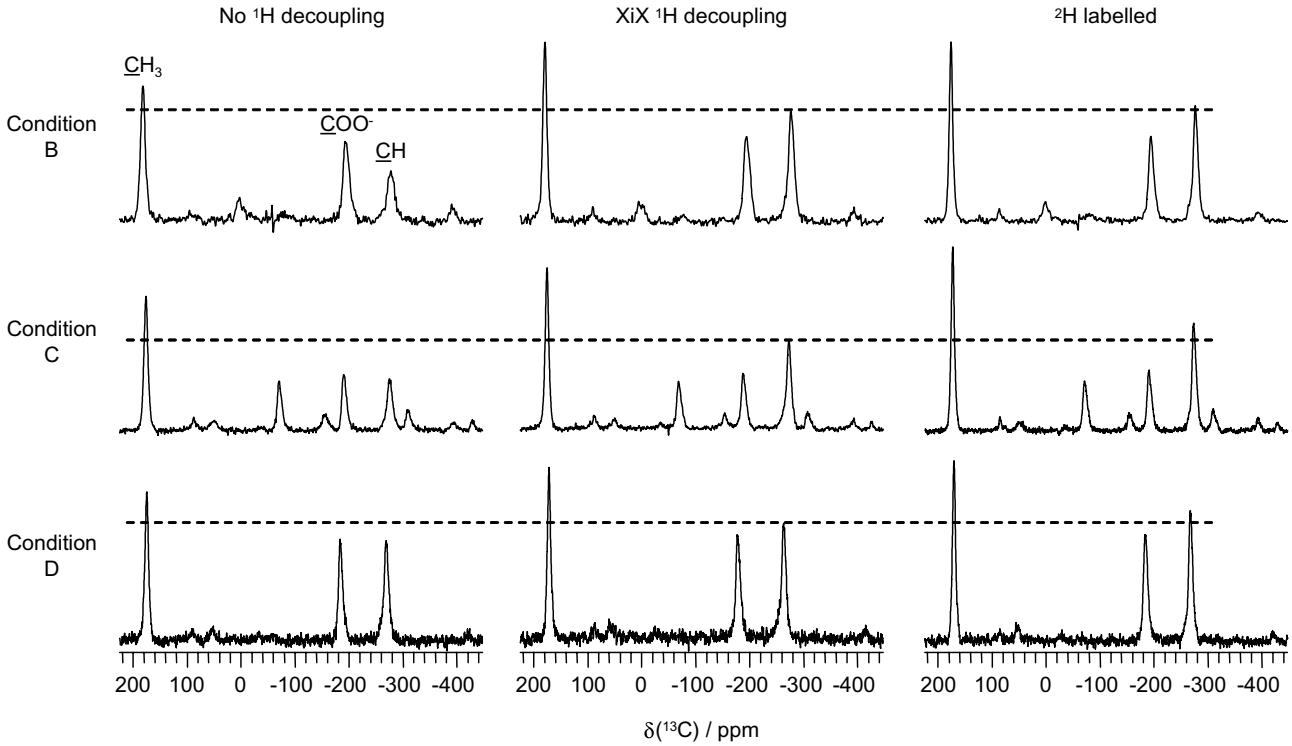

Fig. 4. ^{13}C spin-echo MAS NMR spectra of natural abundance Cu(DL-alanine)$_2$·H_2O acquired without ^1H decoupling (left column), with XiX decoupling (middle column), in comparison to ^{13}C spectra of fully deuterated Cu(DL-alanine)$_2$·D_2O (right column) under condition B (top row), condition C (middle row), and condition D (bottom row). For all spectra, the total experiment time was 2 h 20 min, the interpulse delay was set to 66.67 μs, and FIDs were apodized with 50 Hz line broadening before Fourier-transform. Under conditions B and C, the recycle delay was 1 s, as limited by the duty cycle of the probe, and 8k transients were collected. Under condition D, the recycle delay was limited by the spin–lattice relaxation time of the methyl carbon ($5T_1 = 0.25$ s) and 32 k transients were collected.

decoupling than is the methine group in Cu(ala-2-^{13}C)$_2$·H_2O and displayed some different behaviour (Figs. 5B and 3B, respectively). For example, with CW decoupling under condition A, the methylene carbon signal of Cu(ambut-3-^{13}C)$_2$ increased by a factor of 4.4; much greater than the maximum signal increase observed in Cu(ala-2-^{13}C)$_2$·H_2O under any conditions or with any of the studied decoupling sequences. In addition, under condition A, SPINAL-64 provided the largest signal increase for the methylene group in Cu(ambut-3-^{13}C)$_2$ whereas for the methine group in Cu(ala-2-^{13}C)$_2$·H_2O, SPINAL-64 provided the smallest signal increase of the advanced sequences. The best performance, however, was still observed for XiX decoupling under condition B, where the methylene peak intensity increased by a factor of 28 in comparison to no decoupling. Again, a decrease in ^1H decoupling performance was observed upon moving to 11.75 T (condition C) and under condition D the ^{13}C signal intensity is the least sensitive to ^1H decoupling. At $B_o = 11.75$ T, a decrease in signal was not observed when CW decoupling was used, but CW performed very poorly in comparison to any of the advanced decoupling sequences.

From examination of the ^{13}C NMR spectra of Cu(ambut)$_2$ presented in Fig. 6, the behaviour of the carboxylate carbon peak ($\delta_{iso} = -191$ ppm) and methine carbon peak ($\delta_{iso} = -274$ ppm) is essentially the same as observed for Cu(ala)$_2$·H_2O. For the methylene carbon ($\delta_{iso} = 25$ ppm), in the absence of ^1H decoupling (condition B, top left spectrum of Fig. 6) this NMR peak is barely visible and is masked by the broad spinning sideband of the carboxylate group that is centred about 5 ppm. The considerable increase in the signal-to-noise of the methylene ^{13}C peak observed with XiX decoupling is dramatic, and is improved further upon complete deuteration. Although this peak is very sensitive to ^1H decoupling, the significant increase in peak intensity (35%) for the deuterated sample demonstrates that the ^1H decoupling using XiX decoupling is actually far from perfect.

Upon moving to $B_o = 11.75$ T (condition C, middle row of Fig. 6) the large signal increase for the methylene carbon obtained with ^1H decoupling has already been demonstrated in Fig. 5B (a factor of 12 increase). In comparison to the deuterated sample, it is quite clear that considerable ^{13}C–^1H dipolar interactions between the methylene group carbon and protons are still present as the intensity of the ^{13}C methylene peak nearly doubles upon deuteration. This is a larger increase than observed under condition B, where $B_o = 7.05$ T. At the faster spinning rate, without ^1H decoupling (condition D, bottom row of Fig. 6) the methylene carbon peak is slightly better resolved than with $\nu_{rot} = 15$ kHz, but the benefit of XiX decoupling even with

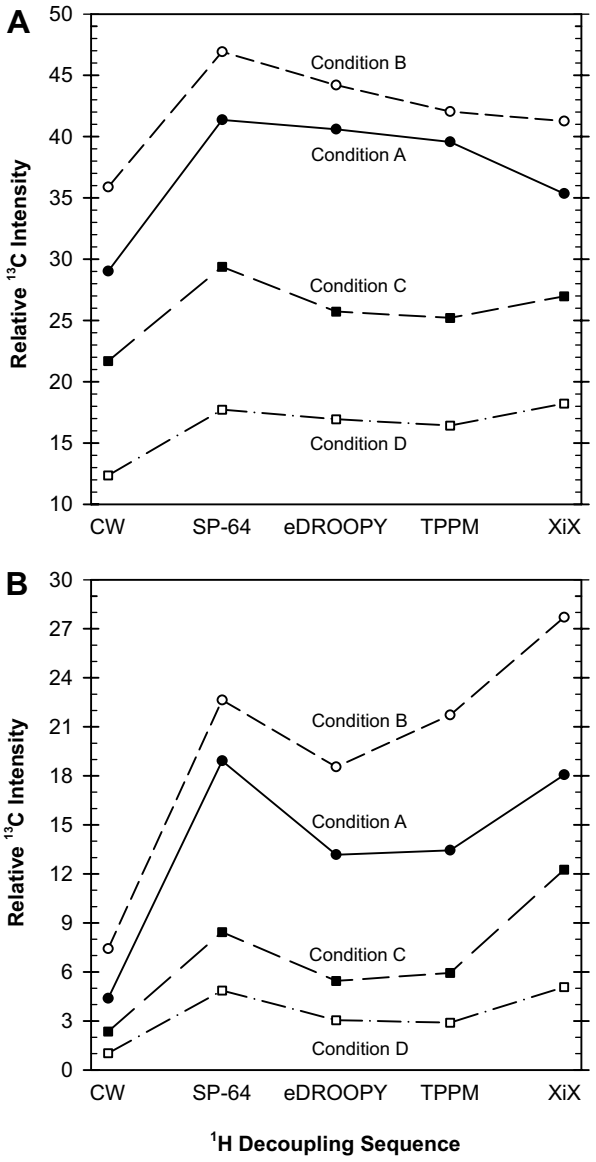

Fig. 5. (A) Plot of ^{13}C signal intensity of the methylene carbon of DL-2-aminobutyric acid and (B) Cu(DL-2-aminobutyrate-3-^{13}C)$_2$ under the experimental conditions outlined in Table 1. The ^{13}C signal intensities for each compound are plotted relative to the ^{13}C signal intensity for that compound obtained without ^{1}H decoupling (set to 1.0).

$\nu_{rot} = 30$ kHz is still quite evident. In comparison to the fully deuterated sample, it is clear that with the higher spinning rate and ^{1}H decoupling power, the methylene group is being decoupled with a higher efficiency. Whereas the methylene carbon peak nearly doubled under condition C upon deuteration, an increase of about 1.4 is observed upon deuteration under condition D.

3.2.2. Influence of ^{1}H decoupling on ^{13}C linewidths

The ^{13}C linewidths at half-heights of Cu(ala-2-^{13}C)$_2$·H$_2$O, Cu(ambut-3-^{13}C)$_2$ and their fully deuterium labelled analogues for the decoupling pulse sequences studied under each experimental condition are presented in Fig. 7. For Cu(ala-2-^{13}C)$_2$·H$_2$O, even where the use of CW decoupling resulted in increases in signal intensity (see Fig. 3B), the use of CW decoupling resulted in *broadening* of the methine carbon ^{13}C peak under all conditions (Fig. 7A). At both magnetic field strengths studied, the broadening was reduced, but not eliminated, by increasing the decoupling field strength. The greatest increase in the linewidths was obtained under condition C, where the linewidth changed from 11.1 ppm in the absence of decoupling to 19.8 ppm with CW decoupling. Under this condition, a decrease in the signal intensity was also observed with CW decoupling (see Fig. 3B). For Cu(ambut-3-^{13}C)$_2$, increases in the linewidths were observed under all but condition B.

Unlike for CW decoupling, for both compounds studied the use any of the advanced decoupling sequences typically resulted in some degree of line narrowing, with XiX decoupling generally resulting in the greatest improvements. With this sequence, any line broadening due to ^{13}C–^{1}H dipolar coupling is removed under conditions B through D, and the linewidths obtained are essentially the same as for the fully deuterium labelled samples. The linewidths obtained with XiX decoupling are still significantly broader than those observed in diamagnetic organic solids, where under condition B, for example, the linewidths of Cu(ala-2-^{13}C)$_2$·H$_2$O and Cu(ambut-3-^{13}C)$_2$ were 12.6 ppm and 3.0 ppm, respectively. While moving to the higher magnetic field strength, the breadth of the ^{13}C NMR peak of the former compound decreased significantly (in ppm), the linewidth remained constant for the latter compound.

3.2.3. Influence of ^{1}H decoupling on ^{13}C coherence lifetimes (T_2')

The coherence lifetime, T_2', is a time constant for the decoherence of transverse magnetization. Under rapid magic-angle spinning and ^{1}H decoupling, the ^{13}C coherence lifetimes are influenced by the nuclear transverse relaxation time, T_2, and residual ^{13}C–^{1}H dipolar coupling [57,64]. Since the latter typically limits the coherence lifetimes in organic solids, the T_2' values are very sensitive to the ^{1}H decoupling sequence utilized. On a practical level, increasing the coherence lifetimes by optimizing ^{1}H decoupling has been shown to result in a significant increase in the sensitivity of multiple-pulse NMR experiments [57]. For such experiments to be performed on paramagnetic solids, where coherence lifetimes are considerably shorter than those observed in diamagnetic solids, the need to maximize coherence lifetimes is even more important. On a more fundamental level, the T_2' values obtained depend more strongly on the ^{1}H decoupling sequence used than either the ^{13}C signal intensities or linewidths [57] and when compared to values obtained for the deuterated samples provide the most effective measure of the ^{1}H decoupling efficiency. For example, under condition B, the measured T_2' value for Cu(ala-2-^{13}C)$_2$·H$_2$O without ^{1}H decoupling was 0.57(1) ms, and increased by 70% to 0.97(2) ms with XiX decoupling. Furthermore, unlike with the signal intensities and linewidths where only minor improvements were observed upon deuteration, the T_2' value with XiX is only

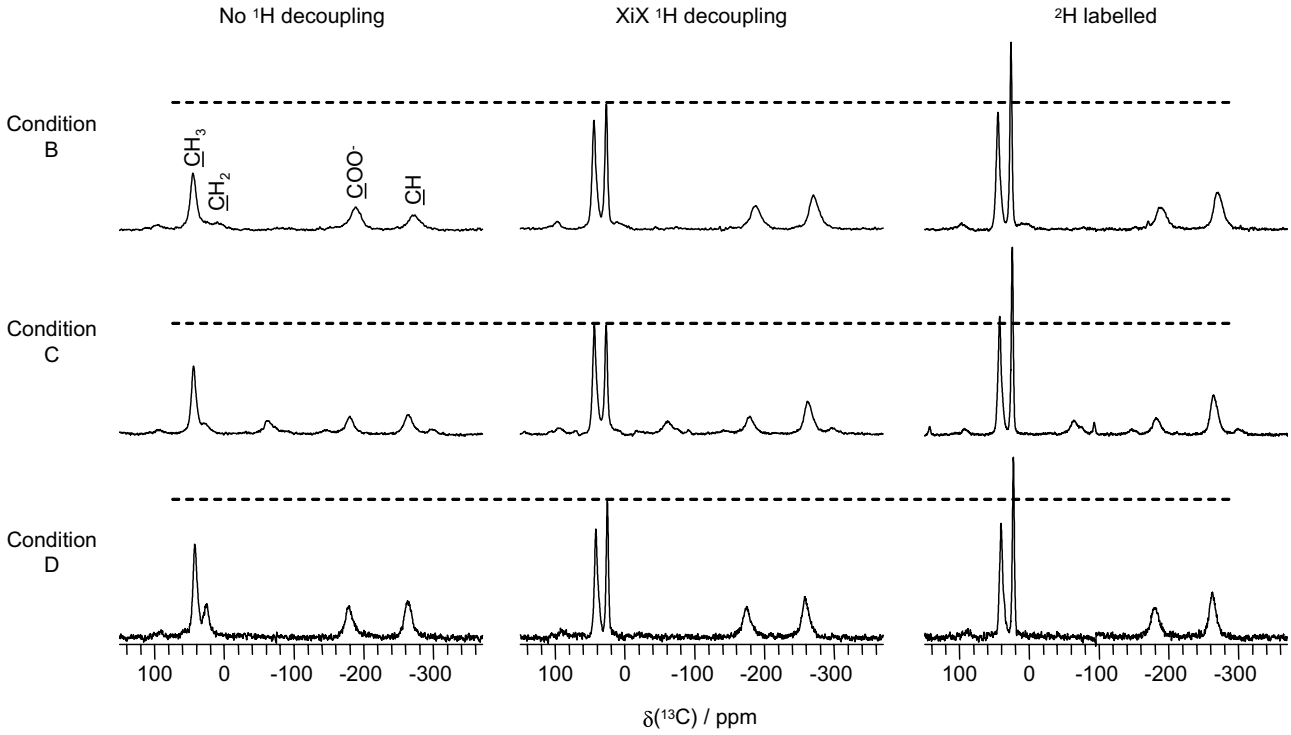

Fig. 6. ^{13}C spin-echo MAS NMR spectra of natural abundance Cu(DL-2-aminobutyrate)$_2$ acquired without ^1H decoupling (left column), with XiX decoupling (middle column), in comparison to ^{13}C spectra of fully deuterated Cu(DL-2-aminobutyrate)$_2$ (right column) under condition B (top row), condition C (middle row), and condition D (bottom row). For all spectra, the total experiment time was 2 h 20 min, the interpulse delay was set to 66.67 μs, and FIDs were apodized with 50 Hz line broadening before Fourier-transform. Under conditions B and C, the recycle delay was 1 s, as limited by the duty cycle of the probe, and 8 k transients were collected. Under condition D, the recycle delay was limited by the spin–lattice relaxation time of the methyl carbon ($5T_1 = 0.35$ s) and 23,056 transients were collected.

about 70% of that for the deuterated sample. Under the same condition, T_2' values for Cu(ambut-3-$^{13}C)_2$ increased dramatically from 0.25(1) ms to 2.7(2) ms with XiX decoupling, and to 13.8(5) ms upon deuteration.

For both compounds, without ^1H decoupling and for the deuterated samples, the T_2' values are essentially unchanged upon moving to the higher magnetic field (condition B and C). This demonstrates that the T_2' values are not field-dependent, which is particularly important because the T_2' values can therefore be used as a quantitative measure of the ^1H decoupling efficiency over different experimental conditions. With that in mind, it is clear that the decreases in the T_2' values obtained with ^1H decoupling upon moving to condition C are due to a drop in the ^1H decoupling efficiency and only with the SPINAL-64 and XiX sequences is decoupling significantly more efficient under condition D than condition B. Even with the most efficient decoupling, the T_2' value for Cu(ala-2-$^{13}C)_2{\cdot}H_2O$ and Cu(ambut-3-$^{13}C)_2$ are about 80% and 35% of the values for the corresponding deuterated compound, respectively.

4. Discussion of results

4.1. Performance of the ^1H decoupling sequences

From the linewidth and intensity data presented above, it is clear that CW decoupling is outperformed by any of the advanced decoupling sequences and is not suitable for use in the ^{13}C NMR of paramagnetic solids. While its use generally resulted in signal increases, any increase was typically offset by a broadening of the NMR peak. This broadening was unexpected, considering that in the diamagnetic solids studied, CW decoupling resulted only in considerable line narrowing. Some insight into why this line broadening occurs and why CW decoupling is outperformed by the advanced decoupling sequences can be drawn from the considerable work that has been done to better understand ^1H heteronuclear decoupling in diamagnetic solids [45,53,58,65–81]; progress on the topic has been recently reviewed [8,9]. In order for ^1H heteronuclear decoupling to be effective, there must be rapid spin-diffusion between the ^1H nuclei. The spin-diffusion causes rapid flip-flop of the ^1H spins and results in "self-decoupling" of the ^1H spins from the ^{13}C spins [65,67,69,74]. Reduction of spin-diffusion rates by increasing the spinning rate [68,74] has been shown to degrade the performance of CW decoupling and the linewidth broadens as the spinning rate increases [58,67,69,70,75]. At spinning rates used in this study, 15 and 30 kHz, the spin-diffusion rate is reduced enough that the performance of CW decoupling is severely degraded in comparison to slower spinning rates. The residual linewidths observed under CW decoupling arise primarily from recoupling of the magnetic shielding anisotropy of the decoupled spins and the heteronuclear dipolar coupling

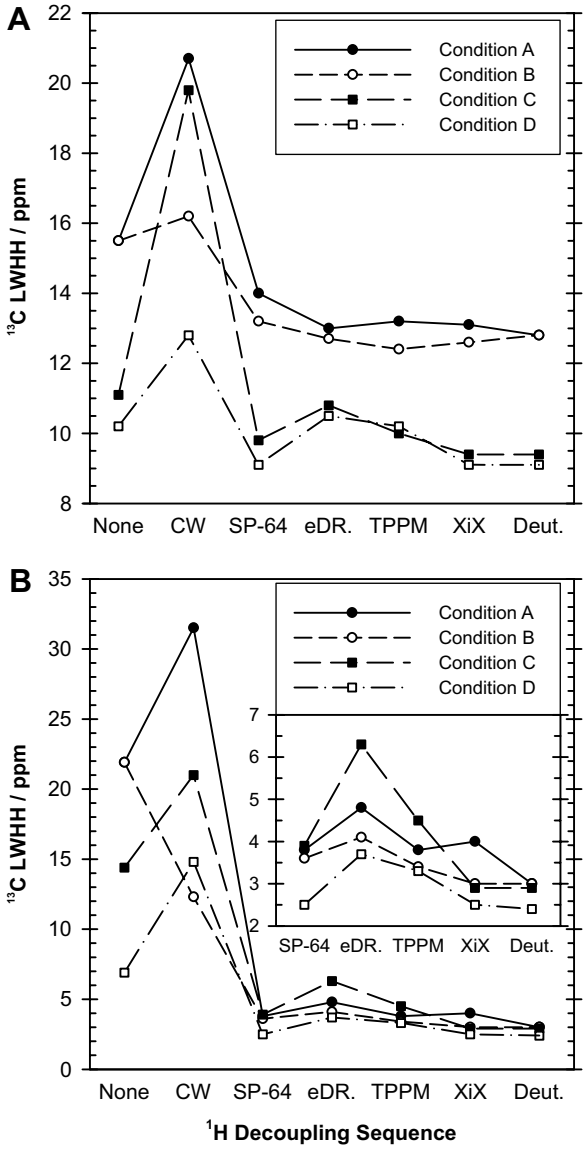

Fig. 7. (A) Plot of the ^{13}C linewidths at half-height, LWHH, of Cu(DL-alanine-2-^{13}C)$_2$·H$_2$O and (B) Cu(DL-2-aminobutyrate-3-^{13}C)$_2$ upon the inclusion of ^{1}H decoupling under the experimental conditions outlined in Table 1.

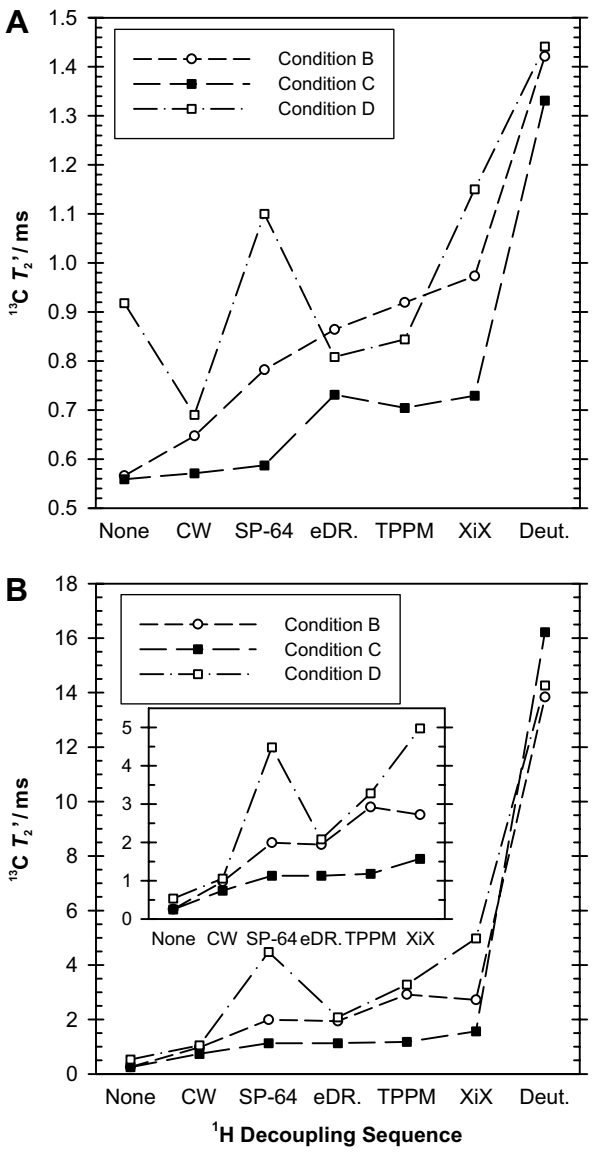

Fig. 8. (A) Plot of the ^{13}C coherence lifetimes, T_2', of Cu(DL-alanine-2-^{13}C)$_2$·H$_2$O and (B) Cu(DL-2-aminobutyrate-3-^{13}C)$_2$ upon the inclusion of ^{1}H decoupling under the experimental conditions outlined in Table 1.

that is no longer averaged by rapid spin-diffusion [45,72,77]. For isolated spin-pairs, this recoupling results in a broad doublet [72,82], the splitting of which, in Hz, depends directly on the magnetic shielding anisotropy of the decoupled spin and hence the magnetic field strength [76], but inversely with the decoupling strength [72,82].

For paramagnetic organic solids, the presence of unpaired electrons indirectly results in an increase in the magnitude of the cross-terms arising from the ^{13}C–^{1}H dipolar coupling and ^{1}H magnetic shielding anisotropy, and thus the residual linewidths observed under CW decoupling. First, the unpaired electrons result in an increase in the effective ^{1}H magnetic shielding anisotropy. Second, the increased ^{1}H chemical shift dispersion that results is believed to reduce the spin-diffusion rate, thus decreasing the self-decoupling of the ^{1}H spins from the ^{13}C spins, and therefore increasing the ^{13}C–^{1}H dipolar coupling interaction. The magnitude of this residual broadening is so large in the paramagnetic solids studied that the use of CW decoupling can actually result in broadening instead of narrowing. The broadening observed behaves as described in the theory, decreasing with increasing decoupling strength (condition A vs. condition B), and increasing upon moving to a higher magnetic field (condition B. vs. condition C).

The advanced decoupling sequences outperform CW decoupling by reducing this broadening caused by the phenomena described above. First, the advanced sequences tend to recouple the ^{1}H–^{1}H homonuclear dipolar interaction, restoring any loss in spin-diffusion due to sample spinning [45,77,78]. As a result, linewidths obtained with

advanced decoupling sequences tend to be essentially independent of the spinning speed used [58,76]. Using average Hamiltonian theory, it has been shown that TPPM reduces the number of the cross-terms between the ^{1}H magnetic shielding anisotropy and the ^{13}C–^{1}H dipolar coupling that dominate the linewidths under CW decoupling [72,77]. Ernst et al. have demonstrated using bimodal Floquet theory that under XiX decoupling, these cross-terms are not present at all and the residual broadening under XiX is due to cross-terms between the homonuclear ^{1}H–^{1}H dipolar coupling and heteronuclear ^{13}C–^{1}H dipolar coupling [81].

Another important consideration is the sensitivity of the ^{1}H decoupling sequence to the large ^{1}H chemical shift dispersion present in paramagnetic organic solids. While in diamagnetic samples all of the advanced decoupling sequences can readily decouple over the entire ^{1}H range, the same may not be true in paramagnetic solids. Therefore, to probe the effect of ^{1}H decoupling bandwidth in paramagnetic samples, we monitored the ^{13}C signal intensity for both Cu(ala-2-^{13}C)$_2$·H$_2$O and Cu(ambut-3-^{13}C)$_2$ as the ^{1}H decoupler frequency was changed. These experiments were performed at $B_o = 7.05$ T with $\nu_{rot} = 15$ kHz and $\nu_1(^1\text{H}) = 100$ kHz (condition B), since these conditions were most sensitive to ^{1}H decoupling, and results are shown in Figs. 9 and 10. Note that "on-resonance" or 0 kHz corresponds to placing the ^{1}H transmitter on the most intense ^{1}H peak, that being the methyl peak at 30 ppm for Cu(ala-2-^{13}C)$_2$·H$_2$O and the methyl peak at 3 ppm for Cu(ambut-3-^{13}C)$_2$.

For the methine peak (Fig. 9), if one considers only the advanced ^{1}H decoupling sequences, the sequence's performance mirrors the sequence's sensitivity offset. For example, XiX has the flattest profile over the ^{1}H transmitter range of 80 kHz, an intensity variation of only 10%, and at all ^{1}H decoupler frequencies provides the greatest signal increase. Conversely, SPINAL-64, which showed the smallest signal increase (see Fig. 3), has the greatest sensitivity to the placement of the ^{1}H transmitter (60% variation). At the extremes, a decrease in signal intensity relative to the ^{13}C peak obtained without ^{1}H decoupling is actually obtained. When considering only the advanced sequences, there definitely seems to be a relationship between the sensitivity of the ^{1}H decoupling sequence to the decoupler frequency and that sequence's performance. Continuous-wave decoupling; however, does not follow this trend as this sequence is very insensitive to the ^{1}H transmitter, actually less so than XiX decoupling, but performs much worse than any of the advanced decoupling sequences when near resonance for the reasons discussed above.

The decoupler frequency experiments presented in Fig. 9 also provide insight into the optimal transmitter placement for maximum decoupling performance. In diamagnetic solids, the ^{1}H chemical shift dispersion is small (~10 ppm) and the ^{1}H transmitter is always placed in the centre of the ^{1}H spectrum, which may or may not be resolved depending on the spinning rate and magnetic field strength, for maximum decoupling performance. Due to the large chemical shift dispersion in paramagnetic solids, however, the ^{1}H transmitter placement is not as obvious. As demonstrated in Fig. 1, the most intense peak in the ^{1}H NMR spectrum of Cu(ala)$_2$·H$_2$O is not in the centre of the spectrum and it is difficult to set the ^{1}H transmitter *a priori*

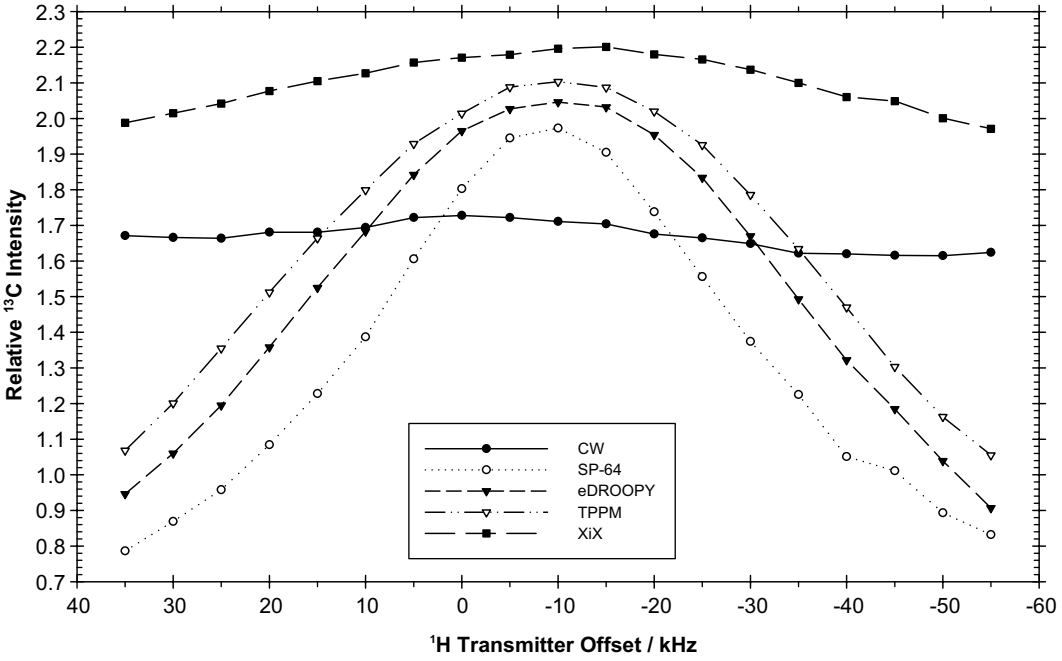

Fig. 9. Plot of the ^{13}C signal intensity of Cu(DL-alanine-2-^{13}C)$_2$·H$_2$O at $B_o = 7.05$ T with various ^{1}H decoupler offsets for the ^{1}H decoupling sequences included in this study. The ^{13}C signal intensities are plotted relative to the ^{13}C signal intensity obtained without ^{1}H decoupling (set to 1.0) and 0.0 kHz represents the transmitter being placed on the most intense ^{1}H peak.

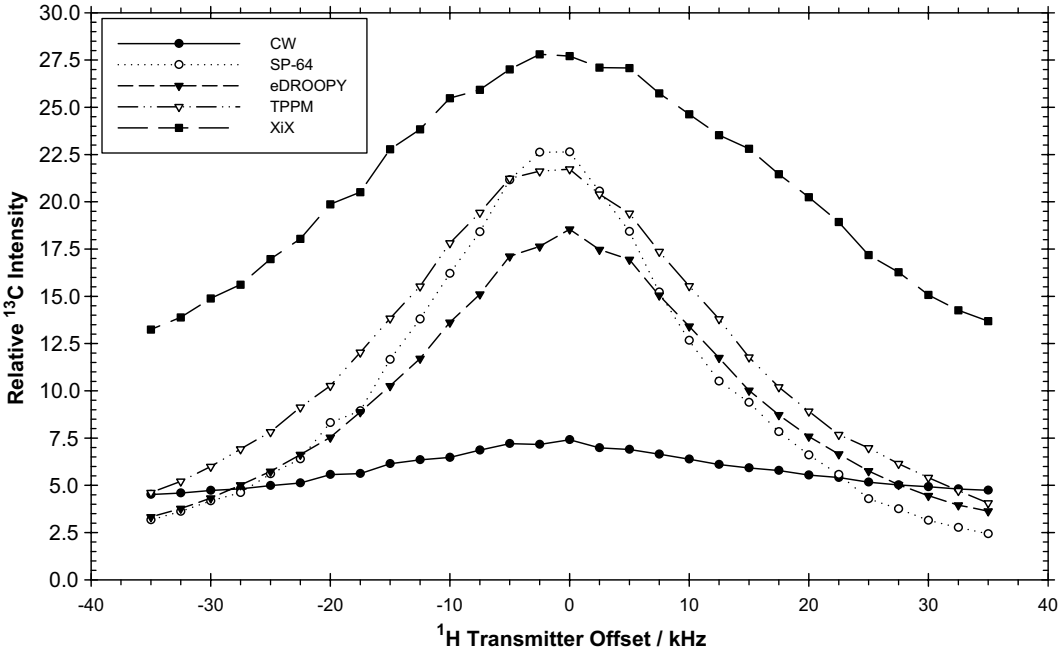

Fig. 10. Plot of the ^{13}C signal intensity of Cu(DL-2-aminobutyrate-3-^{13}C)$_2$ at $B_o = 7.05$ T for various ^{1}H decoupler offsets for the ^{1}H decoupling sequences included in this study. The ^{13}C signal intensities are plotted relative to the ^{13}C signal intensity obtained without ^{1}H decoupling (set to 1.0) and 0.0 kHz represents the transmitter being placed on the most intense ^{1}H peak.

to get the most efficient ^{1}H decoupling. For simplicity, the ^{1}H transmitter was considered "on-resonance" when placed on the most intense peak, although the most efficient ^{1}H decoupling for this sample is actually observed when the ^{1}H transmitter is 10 kHz to low-frequency of the most intense peak.

For the methylene group in Cu(ambut-3-^{13}C)$_2$, slightly different behaviour is observed than in the methine group of Cu(ala-2-^{13}C)$_2$·H$_2$O. Although XiX decoupling provides the most efficient decoupling for all offsets studied, when on-resonance SPINAL-64 outperforms the remaining decoupling sequences, although the SPINAL-64 sequence is the most sensitive to the ^{1}H transmitter offset (Fig. 10). Differences between signal intensities when the ^{1}H transmitter is on-resonance and far from resonance are 39%, 52%, and 89% for CW, XiX, and SPINAL-64 decoupling, respectively. This result seems to suggest that the methylene group is behaving more "diamagnetic", and the performance of the decoupling sequence depends less on the offset sensitivity than the methine group discussed above. This being said, it is quite obvious that the ^{13}C signal intensity in Cu(ambut-3-^{13}C)$_2$ is much more sensitive to the ^{1}H transmitter offset than in Cu(ala-2-^{13}C)$_2$·H$_2$O. This is likely some consequence of the methylene group being more difficult to decouple than the methine group; the methylene carbon therefore being much more responsive to ^{1}H decoupling. The same is observed for diamagnetic solids, where the ^{13}CH$_2$ intensity of glycine is much more sensitive to the ^{1}H transmitter offset than the ^{13}CH of alanine [9]. Furthermore, unlike in Cu(ala-2-^{13}C)$_2$·H$_2$O, maximum ^{1}H decoupling efficiency is observed when the ^{1}H transmitter is placed on the most intense peak in the ^{1}H NMR spectrum. Examination of the ^{1}H NMR spectrum of Cu(ambut)$_2$ presented in Fig. 2, provides some rationale for this observation. The majority of the ^{1}H NMR signal is contained within the most intense ^{1}H peak, less spread out than in Cu(ala)$_2$·H$_2$O and suggests that the ^{1}H resonance of the methylene group, which could not be conclusively assigned earlier, is likely the shoulder to the most intense ^{1}H peak.

4.2. Relative sensitivity of the methine and methylene carbon sites to ^{1}H decoupling

From the data presented in the previous section, ^{1}H decoupling is clearly effective in the ^{13}C MAS NMR of the studied paramagnetic metal-organic solids, provided an advanced ^{1}H decoupling pulse sequence is utilized. By comparing the signal intensities, linewidths, and coherence lifetimes obtained with ^{1}H decoupling to those obtained for fully deuterated analogues, a measure of the ^{1}H decoupling efficiency, or the degree at which the ^{13}C–^{1}H dipolar interactions are being averaged, can be obtained. From this data, it is clear that despite the large spread of ^{1}H resonances (see Figs. 1 and 2), ^{1}H decoupling is efficient in the paramagnetic metal-organic complexes studied, specifically when the XiX decoupling sequence is used. The data suggests that ^{1}H decoupling is, as expected, more efficient in Cu(ala-2-^{13}C)$_2$·H$_2$O than Cu(ambut-3-^{13}C)$_2$. For example, for Cu(ambut-3-^{13}C)$_2$ under condition B, in comparison to the spectrum acquired with XiX decoupling (Fig. 4), an insignificant increase in signal intensity is observed upon deuteration, suggesting nearly ideal decoupling efficiency. For the aminobutyrate complex, however,

the signal increased by about 35% upon deuteration. Examination of the T_2' values further emphasizes the differences in decoupling efficiency and demonstrates that this parameter is the most sensitive probe of decoupling efficiency. Again, under condition B, the T_2' value increased by about 30% upon deuteration for the alanine complex, but nearly 85% for the aminobutyrate complex. The same trend is repeated under conditions C and D. The linewidths provide the least sensitive probe of decoupling efficiency, as there is a negligible difference in the linewidths obtained with XiX decoupling and upon deuteration for both samples under all conditions.

The above data demonstrates that ^{13}C–^{1}H dipolar interactions are being removed by the ^{1}H decoupling in the paramagnetic complexes studied, albeit more so for Cu(ala-2-^{13}C)$_2$·H_2O than Cu(ambut-3-^{13}C)$_2$. Why then, is the signal intensity in the alanine complex drastically less sensitive to ^{1}H decoupling than the aminobutyrate complex and substantially less than for diamagnetic uncomplexed alanine? The answer, it seems, lies primarily in the observed linewidths, specifically in the relative magnitudes of the various line broadening mechanisms the dictate these linewidths, and how these mechanisms are affected by ^{1}H decoupling. Under rapid MAS, the linewidths of dilute-spin NMR peaks in organic solids are determined by three main sources [57,64,83,84]: i) nuclear transverse relaxation, such that the minimum linewidth that can be obtained in an NMR experiment is equal to $1/\pi T_2$, ii) ^{13}C–^{1}H dipolar coupling interactions, and iii) inhomogeneous broadening due to distributions in chemical shifts that arise from macroscopic fluctuations in the applied magnetic field. Such fluctuations arise from several sources, with the most important resulting from the anisotropic bulk magnetic susceptibility, ABMS, of the sample [83,85]. One must appreciate that the greater the ^{13}C–^{1}H dipolar coupling contribution to the ^{13}C linewidth in the absence of ^{1}H decoupling, the more sensitive that carbon peak will be to ^{1}H decoupling. For diamagnetic organic solids such as alanine, under MAS and in the absence of ^{1}H decoupling, the linewidth is dominated by the ^{13}C–^{1}H dipolar interaction; the methine carbon peak of alanine at 11.75 T is about 4 ppm wide. The inclusion of ^{1}H decoupling removes the majority of this broadening, narrowing the peak by about 95% and concentrating the signal to a peak that is as little as 0.2 ppm broad. The net result being a dramatic gain in signal-to-noise, with the remaining linewidth determined by inhomogeneous broadening.

For paramagnetic organic solids, where the transverse relaxation times are typically much shorter, and ABMS much larger, than in diamagnetic organic solids [85–87], to what extent the ^{13}C–^{1}H dipolar interactions contribute to the linewidths in the absence of ^{1}H decoupling is not known. Using the data presented in Section 3.2.2 (see Fig. 7), this contribution can simply be derived, and is the difference between the linewidth obtained for the protonated sample in the absence of ^{1}H decoupling to the linewidth obtained for the deuterated sample under the same experimental conditions (Table 2). Given that this contribution is completely removed under conditions B through D by XiX decoupling (see Fig. 7), the percent contribution of the ^{13}C–^{1}H broadening to the ^{13}C linewidths determines the sensitivity of the carbon peak to ^{1}H decoupling. For instance, this contribution is the largest under condition B, the condition in which the compounds studied were most sensitive to ^{1}H decoupling, and comprised 86% of the linewidth of Cu(ambut-3-^{13}C)$_2$ and only 19% for Cu(ala-2-^{13}C)$_2$·H_2O. The linewidth contribution and thus the sensitivity to ^{1}H decoupling (see Figs. 3 and 5) are clearly larger for the former compound. For the two diamagnetic carbon sites studied, the ^{13}C–^{1}H dipolar broadening makes up about 95% of the linewidth and the ^{13}C peaks are even more sensitive to ^{1}H decoupling. Even though the ^{13}C–^{1}H dipolar broadening is eliminated for the paramagnetic solids by XiX decoupling, the residual linewidths of 12.6 ppm for Cu(ala-2-^{13}C)$_2$·H_2O and 3.0 ppm for Cu(ambut-3-^{13}C)$_2$ are still relatively broad. From the T_2' values presented in Fig. 8, the linewidths dictated by the T_2' values can be determined. These linewidths are much smaller than the residual linewidths and thus the residual linewidths must be limited by inhomogeneous interactions. As for diamagnetic solids, the inhomogeneous broadening is likely dominated by the ABMS of the sample; however, both

Table 2
Broadening of the ^{13}C linewidths due to ^{13}C–^{1}H dipolar coupling and homogeneous contributions to the linewidths obtained with XiX ^{1}H decoupling[a]

Condition	LWHH(none)	LWHH(deut)	ΔLWHH[b]	ΔLWHH/%[c]	$1/\pi T_2'$(XiX)[d]
Cu(ala-^{13}C)$_2$·H_2O					
B	15.5	12.6	2.9	19	4.3
C	11.1	9.4	1.9	15	3.5
D	10.2	9.1	1.1	11	2.2
Cu(ambut-3-^{13}C)$_2$					
B	21.9	3.0	18.9	86	1.5
C	14.4	2.9	11.5	80	1.6
D	6.9	2.4	4.5	65	0.51

[a] Unless otherwise specified, units are ppm.
[b] ΔLWHH = LWHH(none)-LWHH(deut).
[c] ΔLWHH/ % = 100x(ΔLWHH/LWHH(none)).
[d] Converted to ppm by multiplying by the 1/Larmor frequency.

the magnitude and the anisotropy of the magnetic susceptibility is much larger for paramagnetic solids and thus the broadening due to ABMS is consequently much larger.

Upon moving to $B_o = 11.75$ T (condition C), the broadening due to ^{13}C–^{1}H dipolar coupling is independent of the applied magnetic field strength, while ABMS broadening scales with the applied magnetic field strength. As a result the percent contribution to the linewidth from ^{13}C–^{1}H dipolar broadening, and thus the sensitivity to ^{1}H decoupling, decreases upon moving to condition C. This sensitivity is further decreased by doubling the spinning rate (condition D), as the ^{13}C–^{1}H dipolar interactions are averaged more effectively by the spinning itself. In addition, some of the ABMS broadening is reduced and thus the narrowest peaks, both with and without XiX decoupling, are obtained under this condition.

5. Conclusions

An investigation of ^{1}H heteronuclear decoupling in the ^{13}C MAS NMR spectra of paramagnetic metal-organic solids has been presented. The use of ^{1}H decoupling resulted in significant increases in signal intensity for the methylene carbon of Cu(ambut-3-$^{13}C)_2$ but only minor increases were observed for the methine carbon in Cu(ala-2-$^{13}C)_2{\cdot}H_2O$. An increase in the applied magnetic field strength or rotor frequency resulted in a decrease in the sensitivity of the ^{13}C signal intensity to ^{1}H decoupling; however, increasing the ^{1}H rf-field strength resulted in greater decoupling efficiency. All of the advanced decoupling sequences outperformed CW decoupling, with the XiX pulse sequence consistently providing the greatest increases in signal intensity over all experimental conditions studied. The use of any of the advanced decoupling sequences resulted in significant decreases in the ^{13}C linewidths and increases in the ^{13}C T_2' values. By comparing these values obtained on protonated complexes to those obtained for fully deuterated samples, we have shown that advanced ^{1}H decoupling schemes are quite efficient in paramagnetic solids, and are capable of removing all line broadening due to ^{13}C–^{1}H dipolar coupling in the samples studied.

Acknowledgments

The solid-state NMR group at the University of Alberta is thanked for helpful discussions. Prof. Paul Hodgkinson (University of Durham) is thanked for help with modifications of the eDROOPY minimization routine. M.J.W. thanks the Natural Sciences and Engineering Research Council (NSERC) of Canada, the Alberta Ingenuity Fund, and the University of Alberta for funding. D.N.S. is an Izaak Walton Killam post-doctoral fellow and would like to thank the Alberta Ingenuity Fund and the University of Alberta for funding. R.E.W. is a Canada Research Chair in Physical Chemistry and would like to thank the government of Canada, NSERC, and the Canada Foundation for Innovation for funding. Finally, we thank two anonymous referees for several helpful suggestions.

Appendix A. Supplementary data

^{1}H and ^{2}H MAS NMR spectra of Cu(ala-$d_6)_2{\cdot}D_2O$, and Cu(ambut-$d_8)_2$ acquired under various experimental conditions and a discussion of the ^{1}H isotropic chemical shift assignments. Supplementary data associated with this article can be found, in the online version, at doi:10.1016/j.jmr.2007.11.012.

References

[1] M.J. Duer, Essential techniques for spin-1/2 nuclei, in: M.J. Duer (Ed.), Solid-State NMR Spectroscopy: Principles and Applications, Blackwell Science Ltd., Oxford, UK, 2002, pp. 73–110.
[2] D.D. Laws, H.M.L. Bitter, A. Jerschow, Solid-state NMR spectroscopic methods in chemistry, Angew. Chem., Int. Ed. Engl. 41 (2002) 3096–3129.
[3] A. Pines, J.S. Waugh, M.G. Gibby, Proton-enhanced nuclear induction spectroscopy—Method for high-resolution NMR of dilute spins in solids, J. Chem. Phys. 56 (1972) 1776–1777.
[4] A. Pines, M.G. Gibby, J.S. Waugh, Proton-enhanced NMR of dilute spins in solids, J. Chem. Phys. 59 (1973) 569–590.
[5] E.R. Andrew, A. Bradbury, R.G. Eades, Nuclear magnetic resonance spectra from a crystal rotated at high speed, Nature 182 (1958) 1659.
[6] E.R. Andrew, A. Bradbury, R.G. Eades, Removal of dipolar broadening of nuclear magnetic resonance spectra of solids by specimen rotation, Nature 183 (1959) 1802–1803.
[7] E.R. Andrew, Magic angle spinning in solid-state NMR spectroscopy, Philos. Trans. R. Soc. London, Ser. A 299 (1981) 505–520.
[8] M. Ernst, Heteronuclear spin decoupling in solid-state NMR under magic-angle sample spinning, J. Magn. Reson. 162 (2003) 1–34.
[9] P. Hodgkinson, Heteronuclear decoupling in the NMR of solids, Prog. Nucl. Magn. Reson. Spectrosc. 46 (2005) 197–222.
[10] P.K. Burkert, H.P. Fritz, F.H. Köhler, H. Rupp, Spectroscopic studies in chemistry of solids .5. C-13 NMR contact displacements of paramagnetic metallocenes, J. Organomet. Chem. 24 (1970) C59–C60.
[11] V.P. Chacko, S. Ganapathy, R.G. Bryant, C-13 CP-MAS NMR spectra of paramagnetic solids, J. Am. Chem. Soc. 105 (1983) 5491–5492.
[12] G.C. Campbell, R.C. Crosby, J.F. Haw, C-13 chemical-shifts which obey the Curie law in CP MAS NMR spectra—The first CP MAS NMR chemical-shift thermometer, J. Magn. Reson. 69 (1986) 191–195.
[13] S. Ganapathy, V.P. Chacko, R.G. Bryant, M.C. Etter, Carbon CP-MASS NMR and X-ray crystal-structure of paramagnetic lanthanide acetates, J. Am. Chem. Soc. 108 (1986) 3159–3165.
[14] L.D. Hall, T.K. Lim, Studies of metal sugar complexes in the solid-state by the C-13 NMR CP MAS method, Carbohydr. Res. 148 (1986) 13–23.
[15] J.F. Haw, G.C. Campbell, Temperature-dependent chemical-shifts in C-13 CP MAS spectra of paramagnetic solids, J. Magn. Reson. 66 (1986) 558–561.
[16] T.H. Walter, E. Oldfield, Magic-angle sample-spinning NMR spectroscopy of an antiferromagnetically coupled copper formate dimer, J. Chem. Soc., Chem. Commun. (1987) 646–647.
[17] G.C. Campbell, J.F. Haw, Determination of magnetic and structural properties in solids containing antiferromagnetically coupled metal centers using NMR methods. Magneto-structural correlations in anhydrous copper(II) *n*-butyrate, Inorg. Chem. 27 (1988) 3706–3709.
[18] R. Benn, H. Grondey, U. Kölle, Editing of the CP/MAS spectra of the isomers of $[(\eta^5\text{-}Me_5Cp)Cl_2Ru]_2$ via T_1(H) difference spectroscopy, J. Magn. Reson. 89 (1990) 375–377.

[19] A.N. Clayton, C.M. Dobson, C.P. Grey, High-resolution C-13 MAS NMR spectra of paramagnetic lanthanide complexes, J. Chem. Soc., Chem. Commun. (1990) 72–74.
[20] W.C. Finch, R.D. Gillespie, D. Hedden, T.J. Marks, Organometallic molecule-inorganic surface coordination and catalytic chemistry. In Situ CPMAS NMR delineation of organoactinide adsorbate structure, dynamics, and reactivity, J. Am. Chem. Soc. 112 (1990) 6221–6232.
[21] P. Michel, A. Moradpour, P. Penven, L. Firlej, P. Bernier, B. Levy, S. Ravy, A. Zahab, Ring-strain-modified properties of substituted perylene radical-cation salts. A solid-state C-13 CPMAS NMR study, J. Am. Chem. Soc. 112 (1990) 8285–8292.
[22] G.C. Campbell, J.H. Reibenspies, J.F. Haw, Solid-state NMR studies of magneto-structural correlations in anhydrous copper(II) carboxylates, Inorg. Chem. 30 (1991) 171–176.
[23] C.J. Groombridge, M.J. Perkins, High-resolution NMR of a solid organic free-radical: C-13, H-2 and H-1 magic angle spinning of 4-hydroxy-2,2,6,6-tetramethylpiperidine 1-oxyl (tempol), J. Chem. Soc., Chem. Commun. (1991) 1164–1166.
[24] P.J. Barrie, C.J. Groombridge, M.C. Grossel, S.C. Weston, Variable temperature MAS NMR studies of the phase-transition in NaTCNQ, J. Chem. Soc., Chem. Commun. (1992) 1216–1218.
[25] M. Basato, G. Favero, A.C. Veronese, A. Grassi, Ligand configuration on weakly paramagnetic (beta-imino carbonyl enolato)nickel complexes: A combined solid-state C-13 NMR and infrared study, Inorg. Chem. 32 (1993) 763–768.
[26] A.R. Brough, C.P. Grey, C.M. Dobson, Paramagnetic ions as structural probes in solid-state NMR: distance measurements in crystalline lanthanide acetates, J. Am. Chem. Soc. 115 (1993) 7318–7327.
[27] K. Liu, D. Ryan, K. Nakanishi, A. McDermott, Solid-state NMR studies of paramagnetic coordination complexes: a comparison of protons and deuterons in detection and decoupling, J. Am. Chem. Soc. 117 (1995) 6897–6906.
[28] J. Blümel, M. Herker, W. Hiller, F.H. Köhler, Study of paramagnetic chromocenes by solid-state NMR spectroscopy, Organometallics 15 (1996) 3474–3476.
[29] J. Chen, F.F. Cai, Q.F. Shao, Z.E. Huang, S.M. Chen, Solid (dibenzo-18-crown-6)KC_{60}: significant enhanced air-stability and appearance of a strong C-13 NMR signal of C_{60}^- below 200 K with an unexpected negative chemical shift, Chem. Commun. (1996) 1111–1112.
[30] F.H. Köhler, X.L. Xie, Vanadocene as a temperature standard for C-13 and H-1 MAS NMR and for solution-state NMR spectroscopy, Magn. Reson. Chem. 35 (1997) 487–492.
[31] A.C. Kolbert, R. Verel, H. DeGroot, M. Almeida, Determination of the spin density distribution in the organic conductor DMTM(TCNQ)(2) with C-13 magic angle spinning NMR, Mol. Phys. 91 (1997) 725–730.
[32] H. Heise, F.H. Köhler, F. Mota, J.J. Novoa, J. Veciana, Determination of the spin distribution in nitronylnitroxides by solid-state H-1, H-2, and C-13 NMR spectroscopy, J. Am. Chem. Soc. 121 (1999) 9659–9667.
[33] T.P. Spaniol, A. Kubo, T. Terao, Resolution enhancement of magic-angle spinning NMR spectra for paramagnetic solids by zero-quantum NMR, Mol. Phys. 96 (1999) 827–834.
[34] M. Crozet, M. Chaussade, M. Bardet, L. Emsley, B. Lamotte, J.M. Mouesca, Carbon-13 solid-state NMR studies on synthetic model compounds of [4Fe-4S] clusters in the 2(+) state, J. Phys. Chem. A 104 (2000) 9990–10000.
[35] G. Fischer, E. Dormann, Spin density distribution of the conduction electrons in diperylene hexafluorophosphate analysed by high-resolution NMR, Eur. Phys. J.B 15 (2000) 21–27.
[36] H. Heise, F.H. Köhler, X.L. Xie, Solid-state NMR spectroscopy of paramagnetic metallocenes, J. Magn. Reson. 150 (2001) 198–206.
[37] H. Heise, F.H. Köhler, M. Herker, W. Hiller, Inter- and intramolecular spin transfer in molecular magnetic materials. Solid-state NMR spectroscopy of paramagnetic metallocenium ions, J. Am. Chem. Soc. 124 (2002) 10823–10832.
[38] Y. Ishii, N.P. Wickramasinghe, S. Chimon, A new approach in 1D and 2D C-13 high-resolution solid-state NMR spectroscopy of paramagnetic organometallic complexes by very fast magic-angle spinning, J. Am. Chem. Soc. 125 (2003) 3438–3439.
[39] T. Jovanovic, A.E. McDermott, Observation of ligand binding to cytochrome P450-BM-3 by means of solid-state NMR spectroscopy, J. Am. Chem. Soc. 127 (2005) 13816–13821.
[40] G. Maruta, S. Takeda, Solid-state high-resolution NMR studies on spin density distribution of a ferromagnetic coordination polymer: Ni(NCS)(2)(Him)(2), Polyhedron 24 (2005) 2424–2430.
[41] G. Kervern, G. Pintacuda, Y. Zhang, E. Oldfield, C. Roukoss, E. Kuntz, E. Herdtweck, J.M. Basset, S. Cadars, A. Lesage, C. Copéret, L. Emsley, Solid-state NMR of a paramagnetic DIAD-Fe^{II} catalyst: sensitivity, resolution enhancement, and structure-based assignments, J. Am. Chem. Soc. 128 (2006) 13545–13552.
[42] N.P. Wickramasinghe, Y. Ishii, Sensitivity enhancement, assignment, and distance measurement in ^{13}C solid-state NMR spectroscopy for paramagnetic systems under fast magic angle spinning, J. Magn. Reson. 181 (2006) 233–243.
[43] A.E. Bennett, C.M. Rienstra, M. Auger, K.V. Lakshmi, R.G. Griffin, Heteronuclear decoupling in rotating solids, J. Chem. Phys. 103 (1995) 6951–6958.
[44] Z. Gan, R.R. Ernst, Frequency- and phase-modulated heteronuclear decoupling in rotating solids, Solid State Nucl. Magn. Reson. 8 (1997) 153–159.
[45] M. Eden, M.H. Levitt, Pulse sequence symmetries in the nuclear magnetic resonance of spinning solids: Application to heteronuclear decoupling, J. Chem. Phys. 111 (1999) 1511–1519.
[46] B.M. Fung, A.K. Khitrin, K. Ermolaev, An improved broadband decoupling sequence for liquid crystals and solids, J. Magn. Reson. 142 (2000) 97–101.
[47] A. Khitrin, B.M. Fung, Design of heteronuclear decoupling sequences for solids, J. Chem. Phys. 112 (2000) 2392–2398.
[48] K. Takegoshi, J. Mizokami, T. Terao, 1H decoupling with third averaging in solid NMR, Chem. Phys. Lett. 341 (2001) 540–544.
[49] A. Detken, E.H. Hardy, M. Ernst, B.H. Meier, Simple and efficient decoupling in magic-angle spinning solid-state NMR: the XiX scheme, Chem. Phys. Lett. 356 (2002) 298–304.
[50] G. de Paëpe, P. Hodgkinson, L. Emsley, Improved heteronuclear decoupling schemes for solid-state magic angle spinning NMR by direct spectral optimization, Chem. Phys. Lett. 376 (2003) 259–267.
[51] G. de Paëpe, D. Sakellariou, P. Hodgkinson, S. Hediger, L. Emsley, Heteronuclear decoupling in NMR of Liquid Crystals using continuous phase modulation, Chem. Phys. Lett. 368 (2003) 511–522.
[52] G. Gerbaud, F. Ziarelli, S. Caldarelli, Increasing the robustness of heteronuclear decoupling in magic-angle sample spinning solid-state NMR, Chem. Phys. Lett. 377 (2003) 1–5.
[53] A.K. Khitrin, T. Fujiwara, H. Akutsu, Phase-modulated heteronuclear decoupling in NMR of solids, J. Magn. Reson. 162 (2003) 46–53.
[54] J. Leppert, O. Ohlenschläger, M. Görlach, R. Ramachandran, Adiabatic heteronuclear decoupling in rotating solids, J. Biomol. NMR 29 (2004) 319–324.
[55] X. Filip, C. Tripon, C. Filip, Heteronuclear decoupling under fast MAS by a rotor-synchronized Hahn-echo pulse train, J. Magn. Reson. 176 (2005) 239–243.
[56] R.S. Thakur, N.D. Kurur, P.K. Madhu, Swept-frequency two-pulse phase modulation for heteronuclear dipolar decoupling in solid-state NMR, Chem. Phys. Lett. 426 (2006) 459–463.
[57] G. de Paëpe, N. Giraud, A. Lesage, P. Hodgkinson, A. Böckmann, L. Emsley, Transverse dephasing optimized solid-state NMR spectroscopy, J. Am. Chem. Soc. 125 (2003) 13938–13939.
[58] G. de Paëpe, A. Lesage, L. Emsley, The performance of phase modulated heteronuclear dipolar decoupling schemes in fast magic-angle-spinning nuclear magnetic resonance experiments, J. Chem. Phys. 119 (2003) 4833–4841.
[59] E.L. Hahn, Spin echoes, Phys. Rev. 80 (1950) 580–594.

[60] H.Y. Carr, E.M. Purcell, Effects of diffusion on free precession in nuclear magnetic resonance experiments, Phys. Rev. 94 (1954) 630–638.
[61] R.K. Harris, A.C. Olivieri, Quadrupolar effects transferred to spin-1/2 magic-angle spinning spectra of solids, Prog. Nucl. Magn. Reson. Spectrosc. 24 (1992) 435–456.
[62] Y.J. Jiang, R.J. Pugmire, D.M. Grant, An efficient double-tuned $^{13}C/^{1}H$ probe circuit for CP/MAS NMR and its importance in linewidths, J. Magn. Reson. 71 (1987) 485–494.
[63] H. Janssen, A. Brinkmann, E.R.H. van Eck, P.J.M. van Bentum, A.P.M. Kentgens, Microcoil high-resolution magic angle spinning NMR spectroscopy, J. Am. Chem. Soc. 128 (2006) 8722–8723.
[64] M.M. Maricq, J.S. Waugh, NMR in rotating solids, J. Chem. Phys. 70 (1979) 3300–3316.
[65] G. Sinning, M. Mehring, A. Pines, Dynamics of spin decoupling in carbon-13-proton NMR, Chem. Phys. Lett. 43 (1976) 382–386.
[66] M. Mehring, G. Sinning, Dynamics of heteronuclear spin coupling and decoupling in solids, Phys. Rev. B 15 (1977) 2519–2532.
[67] I.J. Shannon, K.D.M. Harris, S. Arumugam, High-resolution solid state ^{13}C NMR studies of ferrocene as a function of magic angle sample spinning frequency, Chem. Phys. Lett. 196 (1992) 588–594.
[68] S. Zhang, B.H. Meier, R.R. Ernst, Local monitoring of proton spin diffusion in static and rotating samples via spy detection, Solid State Nucl. Magn. Reson. 1 (1993) 313–320.
[69] P. Tekely, P. Palmas, D. Canet, Effect of proton spin-exchange on the residual C-13 MAS NMR linewidths—Phase-modulated irradiation for efficient heteronuclear decoupling in rapidly rotating solids, J. Magn. Reson. A 107 (1994) 129–133.
[70] T. Nakai, C.A. McDowell, Spinning-frequency-dependent linewidths in ^{1}H-decoupled ^{13}C magic-angle spinning NMR spectra, Chem. Phys. Lett. 227 (1994) 639–644.
[71] J.R. Sachleben, S. Caldarelli, L. Emsley, The effect of spin decoupling on line shapes in solid-state nuclear magnetic resonance, J. Chem. Phys. 104 (1996) 2518–2528.
[72] M. Ernst, S. Bush, A.C. Kolbert, A. Pines, Second-order recoupling of chemical-shielding and dipolar-coupling tensors under spin decoupling in solid-state NMR, J. Chem. Phys. 105 (1996) 3387–3397.
[73] D.B. Zax, Field-dependent isotropic shifts and limitations to linewidths in solid state nuclear magnetic resonance: a Floquet treatment, J. Chem. Phys. 105 (1996) 6616–6625.
[74] M. Ernst, A. Verhoeven, B.H. Meier, High-speed magic-angle spinning C-13 MAS NMR spectra of adamantane: self-decoupling of the heteronuclear scalar interaction and proton spin diffusion, J. Magn. Reson. 130 (1998) 176–185.
[75] D.L. VanderHart, G.C. Campbell, Off-resonance proton decoupling on-resonance and near-resonance—A close look at C-13 CPMAS linewidths in solids for rigid, strongly coupled carbons under CW proton decoupling, J. Magn. Reson. 134 (1998) 88–112.
[76] M. Ernst, H. Zimmermann, B.H. Meier, A simple model for heteronuclear spin decoupling in solid-state NMR, Chem. Phys. Lett. 317 (2000) 581–588.
[77] M. Carravetta, M. Edén, X. Zhao, A. Brinkmann, M.H. Levitt, Symmetry principles for the design of radiofrequency pulse sequences in the nuclear magnetic resonance of rotating solids, Chem. Phys. Lett. 321 (2000) 205–215.
[78] G. de Paëpe, B. Eléna, L. Emsley, Characterization of heteronuclear decoupling through proton spin dynamics in solid-state nuclear magnetic resonance spectroscopy, J. Chem. Phys. 121 (2004) 3165–3180.
[79] M. Ernst, A. Samoson, B.H. Meier, Decoupling and recoupling using continuous-wave irradiation in magic-angle-spinning solid-state NMR: a unified description using bimodal Floquet theory, J. Chem. Phys. 123 (2005) 064102.
[80] R. Ramachandran, V.S. Bajaj, R.G. Griffin, Theory of heteronuclear decoupling in solid-state nuclear magnetic resonance using multi pole-multimode Floquet theory, J. Chem. Phys. 122 (2005) 164503.
[81] M. Ernst, H. Geen, B.H. Meier, Amplitude-modulated decoupling in rotating solids: a bimodal Floquet approach, Solid State Nucl. Magn. Reson. 29 (2006) 2–21.
[82] P. Amornsakchai, P. Hodgkinson, R.K. Harris, NMR studies of P-31, H-1 spin pairs in solid tin(II) phosphite and tin(II) hydrogen phosphate, Mol. Phys. 102 (2004) 877–882.
[83] D.L. VanderHart, W.L. Earl, A.N. Garroway, Resolution in C-13 NMR of organic-solids using high-power proton decoupling and magic-angle sample spinning, J. Magn. Reson. (1969) 44 (1981) 361–401.
[84] M. Alla, E. Lippmaa, Resolution limits in magic-angle rotation NMR spectra of polycrystalline solids, Chem. Phys. Lett. 87 (1982) 30–33.
[85] D.L. VanderHart, Magnetic susceptibility and high resolution NMR of liquids and solids, in: D.M. Grant, R.K. Harris (Eds.), Encyclopedia of Nuclear Magnetic Resonance, John Wiley & Sons, Chichester, 1996, pp. 2938–2946.
[86] S. Ganapathy, R.G. Bryant, C-13 spectral-line broadening in paramagnetic solids, J. Magn. Reson. 70 (1986) 149–152.
[87] A. Kubo, T.P. Spaniol, T. Terao, The effect of bulk magnetic susceptibility on solid state NMR spectra of paramagnetic compounds, J. Magn. Reson. 133 (1998) 330–340.